



# Ultrasensitive electrochemical molecularly imprinted sensor based on AuE/Ag-MOF@MC for determination of hemoglobin using response surface methodology

Sudabe Mandani<sup>1</sup> · Behzad Rezaei<sup>1</sup> · Ali Asghar Ensafi<sup>1</sup> · Parisa Rezaei<sup>2</sup>

Received: 15 February 2021 / Revised: 30 April 2021 / Accepted: 2 June 2021 / Published online: 8 July 2021  
© Springer-Verlag GmbH Germany, part of Springer Nature 2021

## Abstract

Considering the importance of determining the levels of hemoglobin (Hb) as a vital protein in red blood cells, in this work a highly sensitive electrochemical sensor was developed based on a gold electrode (AuE) modified with Ag metal–organic framework mesoporous carbon (Ag-MOF@MC) and molecularly imprinted polymers (MIPs). To that end, the MIP layer was formed on the Ag-MOF@MC by implanting Hb as the pattern molecule during the polymerization. The modified electrode was designed using electrochemical approaches including differential pulse voltammetry (DPV), electrochemical impedance spectroscopy (EIS), and cyclic voltammetry (CV). Using a response level experimental design method, the most important parameters affecting the reaction of the sensing system including pH, incubation time, and scanning rate were optimized. Following the same route, the Hb concentration, pH, temperature, and elution times were optimized to prepare the imprinted polymer layer on the Ag-MOF@MC surface. By exploiting DPV techniques based on the optimal parameters, the electrochemical response of the AuE/Ag-MOF@MC-MIPs for Hb determination was recorded in a wide linear dynamic range (LDR) of 0.2 pM to 1000 nM, with a limit of detection (LOD) of 0.09 pM. Moreover, the Ag-MOF@MC-MIP sensing system showed good stability, high selectivity, and acceptable reproducibility for Hb determination. The sensing system was successfully applied for Hb determination in real blood samples, and the results were compared with those of the standard methods for Hb determination. Acceptable recovery (99.0%) and RDS% (4.6%) confirmed the applicability and reliability of the designed Hb sensing system.

**Keywords** Hemoglobin (Hb) · Molecularly imprinted Ag metal–organic framework mesoporous carbon polymers (Ag-MOF@MC-MIPs) · Differential pulse voltammetry (DPV)

## Introduction

Hemoglobin (Hb), a vital protein in red blood cells, is responsible for transporting oxygen and carbon dioxide between the tissues and lungs [1]. The quaternary structure of the Hb molecule includes four polypeptide strains, and each strain has a heme group [2, 3]. The heme site comprises an iron atom [4] connected to a protoporphyrin (amine ring) circle [5], which is responsible for attachment to oxygen and carbon dioxide [6].

The Hb level is widely used in blood tests as an indicator of various disorders such as thalassemia [7], leukemia [8], heart disease [9, 10], anemia [11], sickle cell disease [12], and extreme blood loss [13]. To date, various methods have been used to detect Hb, including mass spectrometry [14], electrochemistry [15], spectrophotometry [16], high-performance liquid chromatography (HPLC) [17], and fluorimetry [18]. Molecular imprinting of polymers such as artificial antibodies is a technique used to construct target-forming cavities in the polymer structure with memory for the selected molecules to be used in structural characterization [19, 20]. Analytical sensors and biosensors are widely used to quantify various types of biomarkers [21]. Artificial antibodies, with advantages including robustness, easy handling, and stability, are excellent in a wide range of applications including sensors and biosensors [22, 23]. The application of molecularly imprinted sensors based on a metal–organic framework is a novel, attractive research field [24]. Organometallic structures are used

✉ Behzad Rezaei  
rezaei@cc.iut.ac.ir

<sup>1</sup> Department of Chemistry, Isfahan University of Technology, Isfahan 84156–83111, Iran

<sup>2</sup> Department of Medical Laboratory Science, School of Medicine, Isfahan University of Medical Sciences, Isfahan 81745-33871, Iran

extensively in areas including biological products, industry, and agriculture, and are used primarily in the field of health and the environment due to their low toxicity [25, 26].

Metal–organic frameworks (MOF), constructed by assembling metal ions with several organic linkers [27], have been widely used in catalysis [28], energy storage [29], sensors [30], and so on, owing to their exceptionally robust frame, nontoxic nature, luminescence, chemical stability, chemical functionality, large surface area, rich active sites, and various structures [31, 32]. However, there are still some limitations to the application of MOF in the electrochemical sensor field, such as small detection range, low sensitivity, and poor repeatability. Recently, a novel imprinted platform based on microporous MOF has been applied in molecularly imprinted polymer (MIP) electrochemical sensors. These microporous MOF have advantages such as minimal crystal congestion, very high surface area, thermal and chemical robustness, tunable chemical properties, and uniform pore structure [33–35]. There are many imprinted places on the surface of microporous MOF which can be exploited for designing organometallic imprinted structures [36]. Regardless of the application and performance, MOF/MIP systems are prepared in two main forms: molecularly imprinted core–shell nanostructures and molecularly imprinted MOF films [37–40]. Today, MOF/MIP electrochemical sensors have attracted significant attention due to their low cost, simplicity, and speed. These structures have been broadly utilized to determine wide groups of molecules ranging from small molecules to biomacromolecules [24, 41].

As previously mentioned, the Hb level is the most widely used blood parameter for screening patients for the presence of various diseases. For this purpose, in the current study, an electrochemical metal–organic framework microporous imprinted sensor was developed for Hb determination. Achieving desirable selectivity and sensitivity is dependent on the choice of proper components. Metallic silver is a highly suitable material for electrochemical applications due to its electronic and conductive properties [42–44]. Given the excellent properties of Ag-MOF@CM-MIPs, the detection of target molecules (Hb) is carried out with high sensitivity. Therefore, the improved repeatability and signal-to-noise ratio as well as the general current intensity are related to the congestion of imprinted cavities in the MIP layer. Therefore, it is extremely important to develop highly active Ag-based MOF nanomaterials for Hb detection. To this end, the present work focuses on new developments in MIP sensors using Ag-MOF@MC.

The final characteristics of the MIP-based sensing system depend on several factors. The microporous imprinted structures can significantly improve response kinetics, which represents a challenge in the management of sensing systems for fast and in situ analysis. The obtained results reveal that the developed sensor can determine the Hb level in blood samples with high selectivity and sensitivity.

## Experimental

### Materials

Silver nitrate (99%), 2-aminoterephthalic acid (99%), dimethylformamide (DMF, 99.8%), ethanol (99%), (3-aminopropyl)triethoxysilane (APTES, 99%), H<sub>3</sub>PO<sub>4</sub> (99%), urea (99%), NaOH (99%), and tetraethyl orthosilicate (TEOS, 99%) were obtained from Sigma-Aldrich. Hemoglobin (Hb, 99%), bovine serum albumin (BSA, 99%), insulin (INS, 99%), human serum albumin (HSA, 99%) and chicken eggwhite lysozyme (Lyz, 90%) were purchased from Kimia Exir Co. (Tehran, Iran). A fresh redox probe (10 mM of [Fe(CN)<sub>6</sub>]<sup>3-/4-</sup> (1:1), 10 mM of KCl in PBS buffer) was used in all electrochemical tests. To prepare the stock solution of Hb (0.01 mol L<sup>-1</sup>), 0.02 g of Hb was dissolved in PBS (20 mL, pH = 6.0). All aqueous solutions were prepared using deionized (DI) water (18.5 MΩ). The PBS buffer used throughout the work was prepared using H<sub>3</sub>PO<sub>4</sub> and its pH adjusted with NaOH.

### Apparatus

All electrochemical measurements were performed using an Autolab compact potentiostat/galvanostat (model PGSTAT 302N) with GPES [General Purpose Electrochemical System] and FRA [Frequency Response Analysis] software. Field emission scanning electron microscopy (FE-SEM), energy-dispersive X-ray analysis (EDS), and mapping analysis were performed using an FE-SEM instrument (Philips XL30) operating at 25 kV. Transmission electron microscopy (TEM) was carried out using a Philips CM30 TEM operating at 300 kV (Netherlands). A Bruker D8 Advance X-ray diffractometer (using Cu-Kα radiation) was used for recording the X-ray diffraction (XRD) patterns. Attenuated total reflection (ATR) analyses were carried out by Fourier transform infrared spectroscopy using a Bruker Alpha spectrometer (diamond crystal). The pH values of all the solutions were adjusted using a pH meter (Corning, model 140).

### Synthesis of Ag-MOF@MC

For Ag-MOF synthesis, first, 50 mL AgNO<sub>3</sub> (0.02 mM) was transferred into a 250 mL round-bottom flask. Next, 10 mL aminoterephthalic acid (0.2 mM) in DMF was added to the container, and the mixture was refluxed for 2 h. The produced brown precipitate was washed with water and ethanol and dried in a vacuum oven at 60 °C for 4 h.

To produce a mesoporous structure (Ag-MOF@MC) by calcination, Ag-MOF was placed in an oven under a flow of N<sub>2</sub> gas and then brought to 700 °C at a rate of 5 °C/min and kept at this temperature for 2 h.

## Synthesis of Ag-MOF@MC-MIPs and Ag-MOF@MC-NIPs

The MIP layer was coated on the Ag-MOF@MC surface by mixing 500 mg of Ag-MOF@MC and 2 mL of 10% NH<sub>3</sub>. Then a solution containing 10 mg of Hb, 1 μL of APTES, and 4 mL of TEOS was added to the vessel and the obtained mixture was stirred overnight.

In this step, to remove Hb trapped in the MIP structure, a reflux process with solvents [(1:1 v/v) acetonitrile (99.9%)/acetic acid (99.8%)] was used. Hb absorbance at 400 nm was monitored every 30 min for 8 h using a UV-Vis spectrophotometer. After 16 measurements, the Hb concentration reached its lowest level, and no further change in Hb absorbance was noted with further washes. The obtained washed MIP nanoparticles were then dried in an oven at 50 °C for 3 h. A diagram of all the absorbance intensity values against the number of cycles was plotted. Non-imprinted polymer (NIP) nanoparticles were fabricated in the same manner, but Hb was not added to the medium.

## Sensor preparation

Three common electrochemical techniques, namely cyclic voltammetry (CV), differential pulse voltammetry (DPV), and electrochemical impedance spectroscopy (EIS), were used to study all the steps of electrode preparation, characterization, and application. All electrochemical analyses were carried out using Ag/AgCl (single junction, 4 M KCl, micro agar salt bridge), gold electrode (AuE), and Pt as the reference, working, and auxiliary electrodes, respectively. Before each electrochemical test, AuE was polished with paper containing 0.3 μM alumina and then ultrasonically cured in DI water for 15 min. The 10 mM [Fe(CN)<sub>6</sub>]<sup>3-/4-</sup> (1:1) with 10 mM KCl in PBS (pH = 6) solution acted as the redox electrolyte in all studies. CV was applied to scan potentials between -0.5 and 1 V at a scan rate of 100 mV s<sup>-1</sup>. All impedance values were recorded at a potential of +0.2 V in a frequency range of 100 mHz to 100 kHz vs. Ag/AgCl, and a sinusoidal signal was set at 10 mV.

DPV measurements were performed at a modulation time of 0.04 s, interval time of 0.4 s, modulation amplitude of 50.0 mV, and step potential of 8.0 mV. Two milligrams of Ag-MOF@MC-MIPs was dispersed in 2.0 mL of PBS (pH = 6.0) under sonication for 45 min (see Supplementary Information (ESM) Fig. S1). Four microliters of the above suspension was then drop-cast onto the surface of the bare AuE and dried at ambient temperature. For comparison, the Au electrode modified with Ag-MOF@MC-NIPs was prepared via a similar procedure. All electrochemical tests were performed using an Autolab system with GPES and FRA software.

## Electrochemical measurement

The binding of MIPs to Hb was carried out by DPV. Before the analysis, MIPs/AuE were incubated in a Hb sample for 17.5 min at ambient temperature and washed several times with PBS (pH = 6.0). DPV was carried out in PBS (pH = 6.0) containing 10 mM [Fe(CN)<sub>6</sub>]<sup>-3/-4</sup> with 10 mM KCl. The corresponding DPV parameters were set as follows: increment potential of 4.2 mV, amplitude of 55 mV, pulse width of 0.2 s, and pulse period of 0.55 s.

## Experimental design

In the present work, response surface methodology (RSM) via central composite design (CCD) was applied to study the actual factors in MIP preparation and sensor function (ESM section S1).

## Results and discussion

### Characterization of nanocomposites

Reflux washing was repeated until there was no further Hb extraction, which was signaled by no further change in the measured absorbance despite additional refluxing with fresh solvent. In the diagram of Hb absorbance intensity versus the number of elution cycles (ESM Fig. S2), this is signaled by a smooth, horizontal line from the 11th cycle marking the constancy in the lowest absorbance intensity of 0.05 Au.

The step-by-step preparation of AuE/MOF@MC-MIPs is shown in Fig. 1, and The DPV, CV, and EIS curves of bare AuE, AuE/MOF, AuE/MOF@MC-MIPs, and AuE/MOF@MC-NIPs are depicted in Fig. 2a–c, respectively. The electrochemical performance of both Ag-MOF and Ag-MOF-MC was investigated, and it was observed that Ag-MOF and Ag-MOF-MC both increased the CV and DPV current intensity on the AuE, but Ag-MOF-MC had higher activation properties due to its high porosity and increased electronic transitions. Therefore, we used the Ag-MOF-MC as a substrate for fabricating MIP layers for Hb determination. With the formation of a polymer layer on the electrode surface, the current decreases due to the blockage of the electrode surface. In the case of MIPs, due to the presence of a greater number of holes on the polymer surface, the current is higher than with the NIP mode. In the presence of Hb, the holes of the MIPs are blocked, so the electrochemical reaction is inhibited and the current is diminished. When Hb leaves the polymer structure, the observed oxidation and reduced CV current increase sevenfold, which is due to the role of Hb in blocking the electrode surface. The change trend in the resistance of the electrode surface, which was studied by EIS, confirmed the previous results. In the presence of nanostructures that

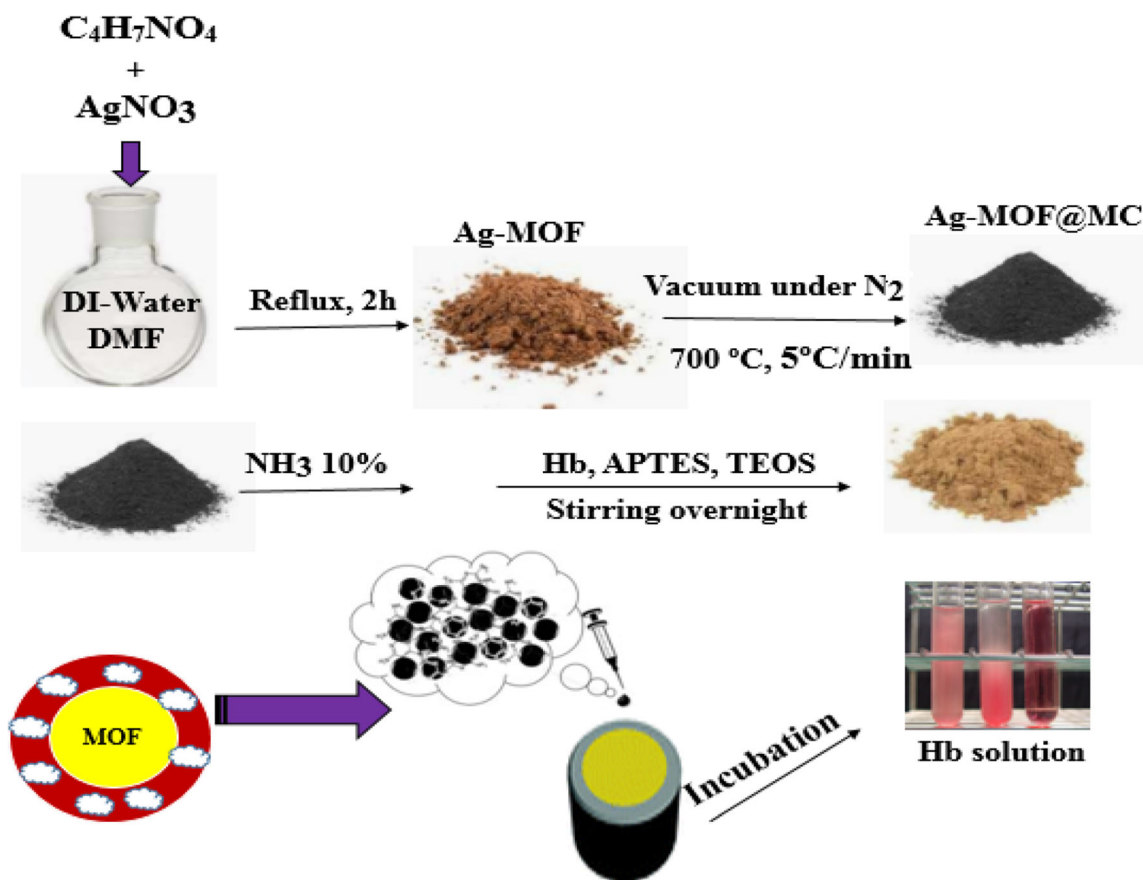


**Fig. 1** Schematic of the step-by-step preparation of AuE/Ag-MOF@MC-MIPs

increase the electron conductivity at the electrode surface, the radius of the EIS semicircle decreased, due to the decreased resistance of the electrode surface.

ATR analysis was performed for all the nanocomposites, and the corresponding spectra are shown in ESM Fig. S3A. In the spectra of Ag-MOF and Ag-MOF@MC, the peaks at  $3400\text{ cm}^{-1}$  and  $1500\text{ cm}^{-1}$  are attributed to the stretching and bending vibrations of the  $\text{NH}_2$  and  $\text{OH}$  groups, respectively. The peaks at  $1423\text{ cm}^{-1}$  and  $1286\text{ cm}^{-1}$  are ascribed to the  $\text{O}-\text{C}-\text{O}$  stretching vibrations, while the bands observed at  $730\text{ cm}^{-1}$  and  $952\text{ cm}^{-1}$  correspond to the vibrational stretching frequencies of the  $(\text{O}-\text{Ag}-\text{O})$  framework. In the spectra of the Ag-MOF@MC-MIPs and Ag-MOF@MC-NIPs, in addition to the similarities, the peaks at  $986\text{ cm}^{-1}$  and  $1136\text{ cm}^{-1}$  correspond to the  $\text{Si}-\text{O}-\text{Si}$  vibrations. Figure S1B (see ESM) shows the XRD patterns of Ag-MOF and Ag-MOF@MC. The X-ray diffraction peaks in the XRD patterns of Ag-MOF and Ag-MOF@MC nanocomposites include the peaks of MOF(Ag) and silver. The reflection peaks of the MOF(Ag) can be attributed to the silver-ATP composite  $\text{Ag}_2(\text{btc})$  (CCDC:198096) [45]. The XRD patterns of Ag-MOF@MC-MIPs and Ag-MOF@MC-NIPs, which show the amorphous structure of the polymer layer and the characteristic peak of Ag-MOF (ESM Fig. S3B), are similar. FE-SEM was used to study the morphology and the particle size

distribution of the nanocomposite. The FE-SEM images of the bare AuE (Fig. 3a), Ag-MOF (Fig. 3b, c), Ag-MOF@MC (Fig. 3d), Ag-MOF@MC-MIPs (Fig. 3e), and Ag-MOF@MC-NIPs (Fig. 3f) are presented in Fig. 3; these images show that the nanocomposites are spherical. The distribution of nanoparticles on the electrode surface was studied by mapping analysis, and the results confirmed the uniformity of particle dispersion (Fig. 3g-j). In addition, average size of 18 nm and 35 nm was estimated for Ag-MOF@MC and Ag-MOF@MC-MIPs, respectively (Fig. 3k, l). The images obtained from the TEM for Ag-MOF@MC-MIPs and Ag-MOF@MC-NIPs (ESM Fig. S4A, B) confirmed the results of the FE-SEM analysis. EDS analysis (ESM Fig. S5) was used to confirm the presence of the desired elements in the Ag-MOF@MC nanocomposite. The sharp Ag peak in the spectrum of this compound confirmed the successful synthesis of Ag-MOF@MC. A set of peaks in the EDS spectrum corresponding to C (7.02%) and Ag (92.98%) were also observed.

### Electrochemical response

The DPV response of the AuE/MOF@MC-MIPs and AuE/MOF@MC-NIPs in the presence of different concentrations of Hb in PBS ( $\text{pH} = 6.0$ ) containing  $10\text{ mM Fe}(\text{CN})_6^{-3/-4}$  with



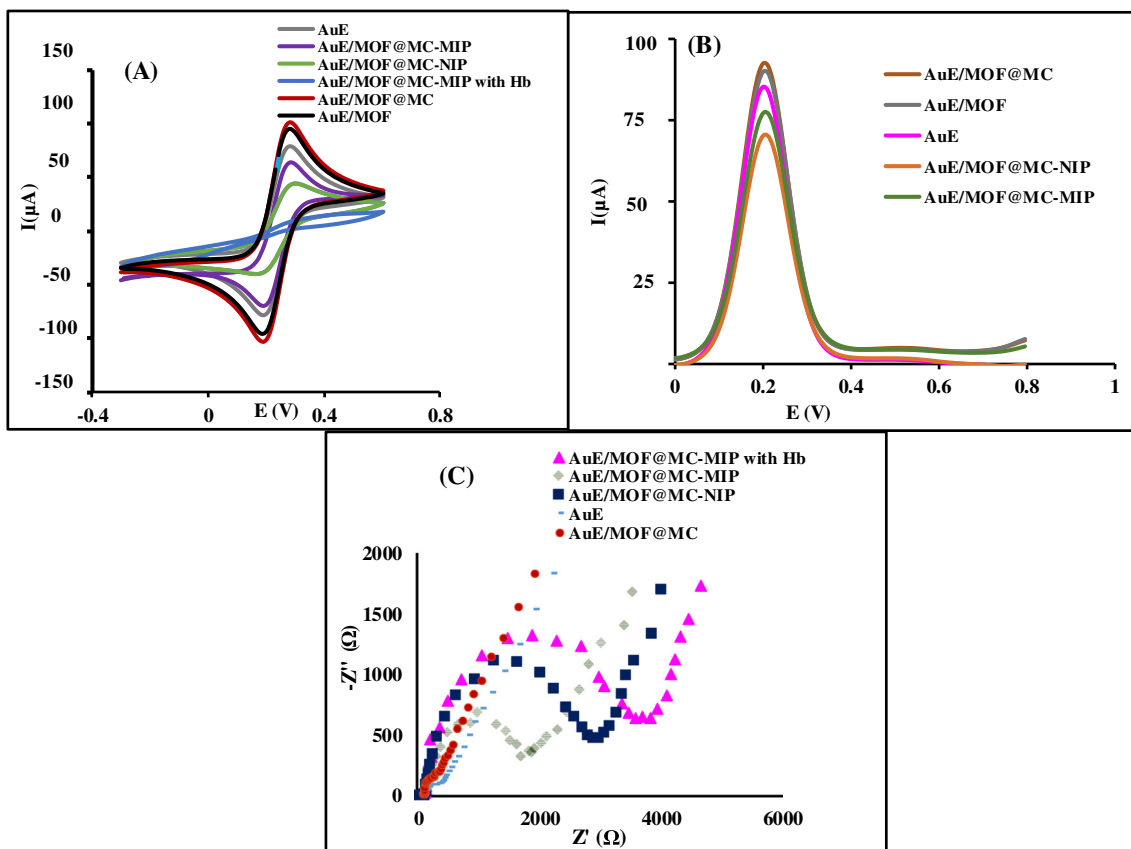


Fig. 2 (a) DPV, (b) CV, and (c) EIS curves of AuE bare, AuE/Ag-MOF, AuE/Ag-MOF@MC, AuE/Ag-MOF@MC-MIPs, and AuE/Ag-MOF@MC-NIPs in a solution containing 10 mM  $[Fe(CN)_6]^{3-/4-}$  (1:1) mixture and 0.1 M KCl in PBS (pH = 6.0)

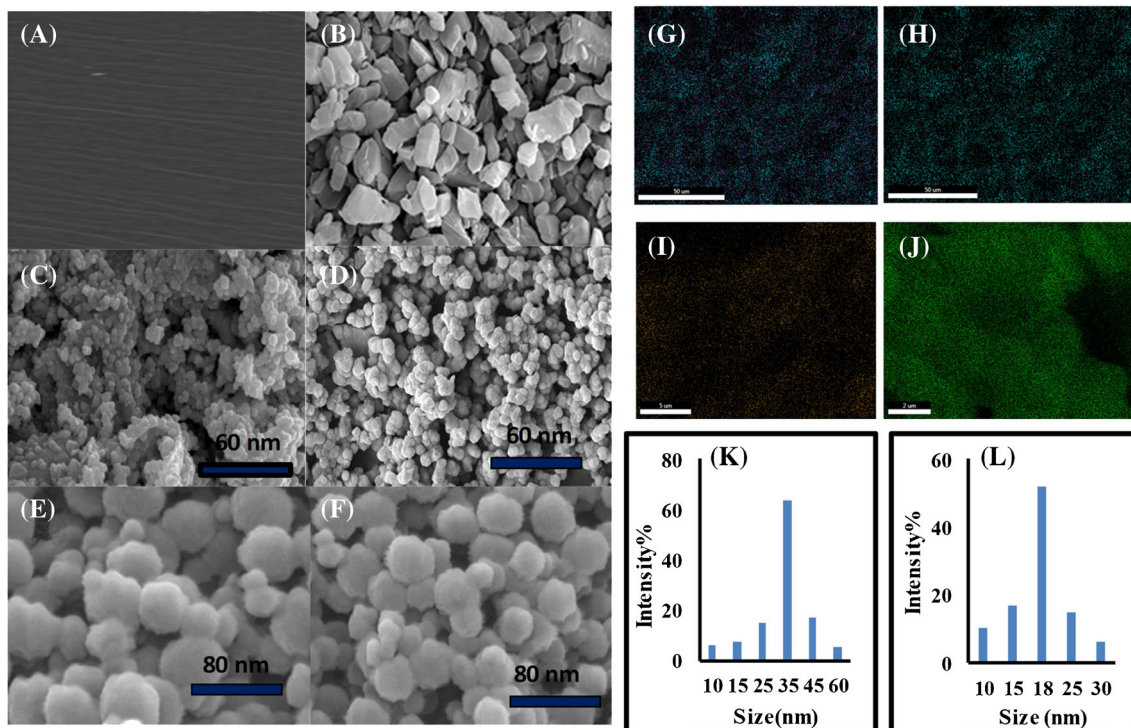
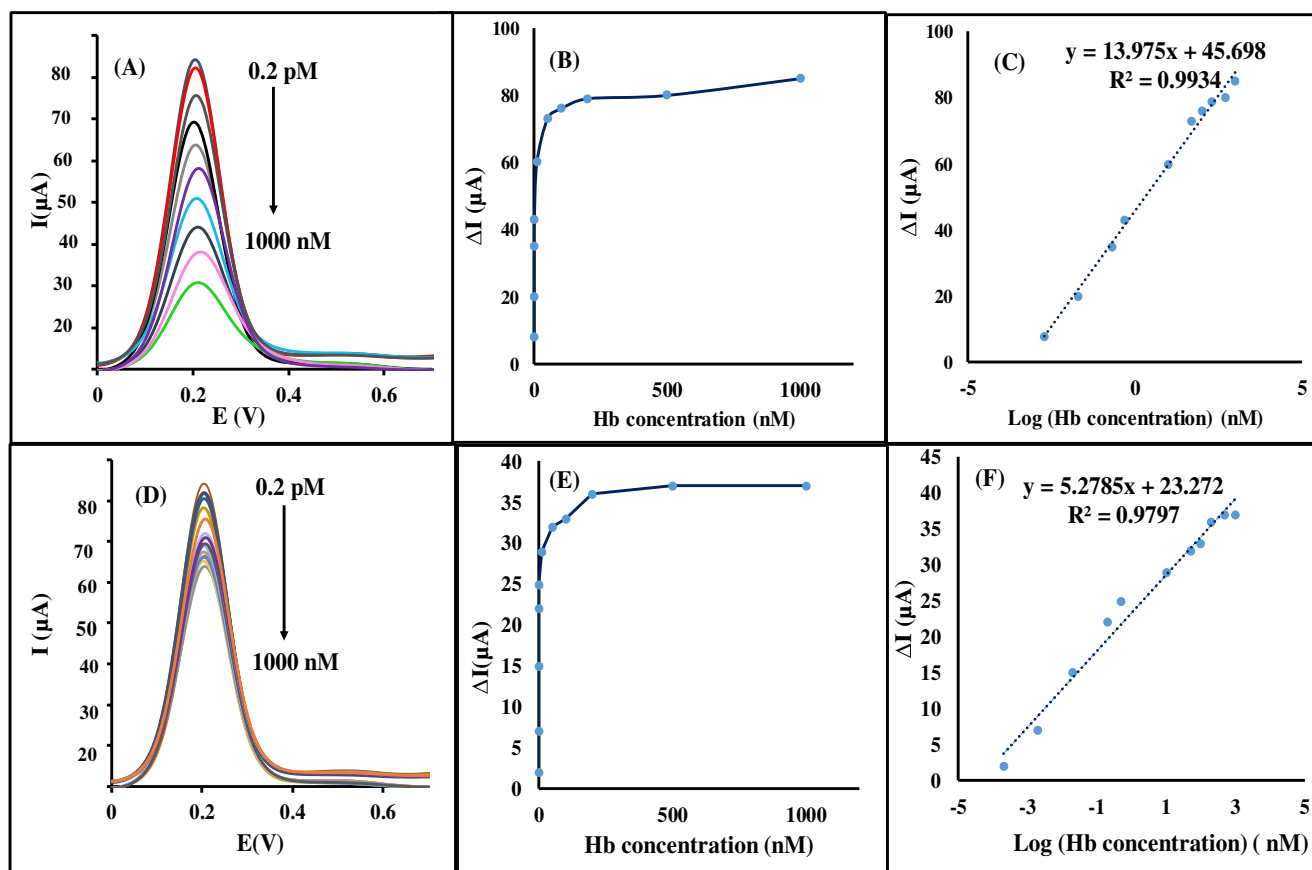


Fig. 3 FE-SEM images of bare AuE (a), Au-MOF (b, c), Ag-MOF@MC (d), Ag-MOF@MC-MIPs (e), and Ag-MOF@MC-NIPs (f). Mapping profile of thin layer of Ag-MOF (g), Ag-MOF-MC (h), Ag-MOF-MC/MIPs (i), and Ag-MOF@MC-NIPs (j) on the AuE surface. Size distribution profile of thin layer of Ag-MOF (g), Ag-MOF-MC (h), Ag-MOF-MC/MIPs (i), and Ag-MOF@MC-NIPs (j)

Size distribution profile of Ag-MOF-MC (k) and Ag-MOF@MC-NIPs (l)



**Fig. 4** (a) DPV voltammograms of proposed AuE/Ag-MOF@MC-MIPs in a solution containing 10 mM  $[\text{Fe}(\text{CN})_6]^{3-/4-}$  (1:1) mixture and 0.1 M KCl in PBS (pH = 6.0) with incubation time = 17.5 min for different concentrations of Hb within a range of 0.2 pM to 1000 nM. Calibration curve for (b)  $\Delta I$  and (c)  $\Delta I$  vs.  $\log(C_{\text{Hb}}, \text{nM})$ . (d) DPV voltammograms of proposed AuE/Ag-MOF@MC-NIPs in a solution containing 10 mM

$[\text{Fe}(\text{CN})_6]^{3-/4-}$  (1:1) mixture and 0.1 M KCl in PBS (pH = 6.0) with incubation time = 17.5 min for different concentrations of Hb from 0.2 pM to 1000 nM. Calibration curve for (e)  $\Delta I$  and (f)  $\Delta I$  vs.  $\log(C_{\text{Hb}}, \text{nM})$ . In all,  $\Delta I$  is the difference between the initial DPV current in the absence of Hb ( $I_0$ ) and the DPV current after the addition of different concentrations of Hb (I)

10 mM KCl was examined. As shown in Fig. 4a, the DPV signal was reduced in the presence of Hb. The corresponding calibration curves with an acceptable value of  $R^2 = 0.99$  are shown in Fig. 4b and c. The DPV curve of the AuE/MOF@MC-NIPs is also shown in Fig. 4d, which shows slight

differences in various concentrations of Hb compared to the MIP response. The corresponding calibration curves are depicted in Fig. 4e and f.

### Optimization of MIP preparation

Four vital parameters, namely, pH (A), Hb concentration (B), temperature (C), and elution times (D), were carefully chosen as the most important parameters affecting the quality of the MIPs and thus the performance of the designed sensor (Table 1). Based on the obtained data, the resulting models acceptably represent the empirical records, with  $R^2$  of 0.99. The F-value of the model was 140.44, indicating the significance of the model. The lack-of-fit (LOF) value obtained was 0.57, indicating that the model is fitted to the whole data, as shown by the results in Table 2. The correlation between the coded parameters and the response was modeled using Eq. (4). The coefficients are recorded in Table 2. R-squared

**Table 1** Variables, their levels and symbols for the CCD in MIP preparation

Variable	Symbol	Level			
		$-\alpha$	-1	+1	$+\alpha$
pH	A	2	4	8	10
Hb concentration (mg/L)	B	0.5	1.5	0.01	2
Temperature ( $^{\circ}\text{C}$ )	C	21.25	33.75	15	40
Elution times (min)	D	6.5	15.5	2	20

**Table 2** The significance possibility (p value; F-value) of regression coefficients, in the predicted second-order polynomial models of the relationship between response and independent variables for MIP preparation

	Linear effects				Interaction effects				Quadratic effects				Model	R <sup>2</sup>		
	A	B	C	D	AB	AC	AD	DC	BD	CD	A <sup>2</sup>	B <sup>2</sup>			C <sup>2</sup>	D <sup>2</sup>
Regression coefficient	19.80	23.46	38.1	218.98	0.12	0.12	20.76	28.75	48.2	9.4	225.3	315.3	104.2	89.7	80.68	0.99
p value; probe >F	<0.0001	<0.0001	<0.0001	<0.0001	<0.65	0.0001	<0.0001	<0.0001	<0.0001	0.0008	<0.0001	<0.0001	<0.0001	<0.0001	<0.0001	<0.0001
F-value	34.46	40.84	67.04	381.19	0.21	23.50	36.14	50.05	83.83	16.41	392.33	548.92	181.35	156.1	140.4	

(0.9998), adjusted R-squared (0.9992), and predicted R-squared (0.9482) were also calculated. In addition, a standard deviation (S.D.) of 0.17, coefficient of variation (CV) of 8.48%, and prediction error sum of squares (PRESS) of 58.47 were obtained. A ratio of greater than 4.0 for an adequate precision value of 34.021 indicates an excellent signal-to-noise (S/N) ratio.

The obtained results were studied using contour plots in the range of the selected variables. The interaction between the Hb concentration and pH is illustrated in Fig. 5a. As shown in Table 2, unlike pH, the Hb concentration had a negative linear effect on the current. The proper concentration of Hb added directly affects the number of complementary sites on the polymer structure. At high concentrations of Hb, the polymer surface is saturated, and excess Hb may block the sites and reduce the quality of the MIPs. At highly acidic and highly basic pH, the MIPs are not stable and thus do not produce a proper electrochemical signal. The effects of temperature and pH on the current are depicted in Fig. 5b. The statistical results (Table 2) show that the linear term of temperature had a greater effect on the response than the pH. Moreover, the interaction between temperature and pH had a positive effect on the signal. As indicated in this figure, the current increased when the pH and temperature values increased to their appropriate ranges. The behavior of the elution times is the same as that presented in Fig. 5c. The simultaneous effects of elution time and pH on the response are shown in Fig. 5c. As shown in Table 2, this interaction is affected by a positive sign, and therefore a significant increase in the response is observed by increasing the elution time. Increasing the elution time due to greater Hb extraction increases the density of the complementary cavities, which has a direct effect on enhanced MIP response to Hb.

The simultaneous effects of Hb concentration and temperature on the response are shown in Fig. 5d. As observed in Table 2, this interaction is affected by a positive sign, and thus an enhanced response is observed by increasing the Hb concentration and temperature to adequate values. The simultaneous effects of the Hb concentration and the elution times on the response are shown in Fig. 5e. As shown in Table 2, the simultaneous effect of these two parameters on the answer obtained has a negative sign, and thus a significant increase in the response is observed by increasing the elution time. However, increasing Hb to a certain concentration increases the current, while a further increase in concentration reduces the response. The concurrent effects of the elution time and the temperature on the current are shown in Fig. 5f. As shown in Table 2, this interaction is affected by a negative sign. Therefore, a significant enhancement in the response is detected by increasing the elution time while the proper value of the temperature is favorable. Finally, using this optimization, the optimal conditions of the MIP preparation were obtained as temperature = 27.5 °C, elution time = 11, pH = 6.0, and Hb concentration = 1.0 (mg/L).

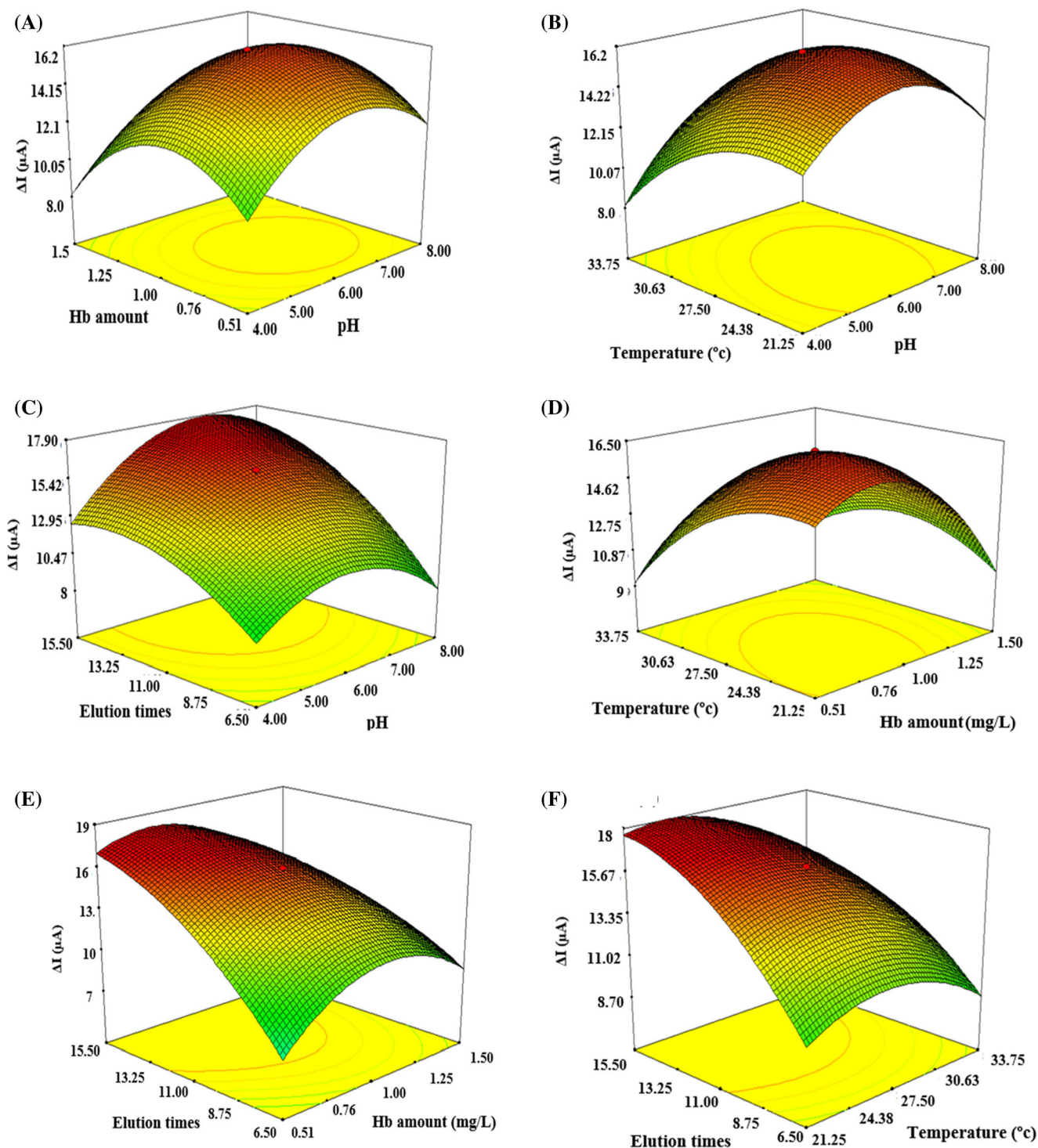


**Fig. 5** The effects of parameters on MIP synthesis. The simultaneous effects of (a) Hb concentration (0.01–2 mg/L) and pH (2–10), (b) temperature (15–40  $^{\circ}\text{C}$ ) and pH (2–10), (c) elution time (2–20) and pH (2–10), (d) temperature (15–40  $^{\circ}\text{C}$ ) and Hb concentration (0.01–2 mg/L),

(e) elution time (2–20) and Hb concentration (2–10), (f) elution time (2–20) and temperature (15–40  $^{\circ}\text{C}$ ). In all,  $\Delta I$  is the difference between the initial DPV current in the absence of Hb ( $I_0$ ) and the DPV current in the presence of 0.02 nM of Hb ( $I$ )

### Optimization of electrochemical response

Three basic parameters of scan rate (E), pH (F), and the incubation time of the probe in the Hb (G) in the electrochemical

trials were selected as the key parameters affecting the behavior of the electro-sensing system. Table S2 (see ESM) shows these parameters and their various levels. The design with 23 experiments represents nine repeats of the focal point, eight



factorial points, and six axial points at an interval of  $\pm 1.6$  from the center. Table S3 (see ESM) shows the results of the analysis of variance (ANOVA) test. According to the obtained data, the resulting models can sufficiently represent the experimental records, with an  $R^2$  of 0.99. The F-value of the model was 199.78, indicating the significance of the model. However, the obtained LOF F-value of 4.74 showed that the model is fitted to all data. According to the results (ESM Table S3), the linear effects of pH, scan rate and incubation time on current changes are positive. Increasing the pH and scanning rate to obtain the optimal values increases the current intensity. Because of the stability of the protein under natural conditions, the best pH for electrode performance is close to neutral pH. Furthermore, at a scan rate of 105 mV/s, the sensor displays its best response (ESM Fig. S6A). As is clear in ESM Fig. S6B, the interaction between the scan rate and incubation time had a negative effect on the response. With a further increase in incubation time, because of the saturation of sites with Hb, changes in current will be negligible. Figure S6C (see ESM) shows the effect of the interaction between the incubation time and pH on current changes. As pointed out, at near-neutral pH and increasing incubation time of 17.5 min, the greatest corresponding current-related changes are observed.

Considering the overall results from the optimization study, the subsequent experimental conditions were selected as follows: incubation time = 17.5 min, scan rate = 105 mV/s and pH = 6.0. The effect of scan rate on electrode performance and active surface calculations of the developed electrodes is described in ESM section S2 (ESM Fig. S8).

## Reproducibility and stability of the sensor

To estimate the reproducibility of the sensor, ten parallelly prepared AuE/MOF@MC-MIP sensors were used for measuring 0.2 pM Hb (PBS, pH = 6.0). Values of  $\Delta I$  for these measurements have a relative standard deviation (RSD) of 2.71%. Three measurements were replicated on one sensor, with RSD calculated for this study indicating good repeatability of sensor performance (ESM, Section S3, Table S1). The storage stability of the prepared AuE/MOF@MC-MIPs may present an important issue during practical applications of Hb determination. The time-dependent current intensity relative to the original signal for 0.2 pM Hb (PBS, pH = 6.0) solution on the first day is shown in Fig. 6a. Between measurements on different days, sensors were maintained at 4 °C under dry conditions. The results confirm that over a period of 45 days, the response for 0.2 pM Hb (PBS, pH = 6.0) is 92.8% of the initial signal (Fig. 6a). This indicates the good storage stability of the AuE/MOF@MC-MIPs.

## Sensor selectivity

The MIPs were formed after the silicon thin film produced when TEOS hydrolyzed on the MOF@MC surface and the copolymerization of the cross-linkers and functional monomers with Hb molecules was completed. In the MIP formation process, functional monomers and Hb molecules interact via reversible covalent or non-covalent bonds. The functional groups of the Hb molecule surrounded by functional monomers are then fixed by a cross-linker. When Hb molecules are

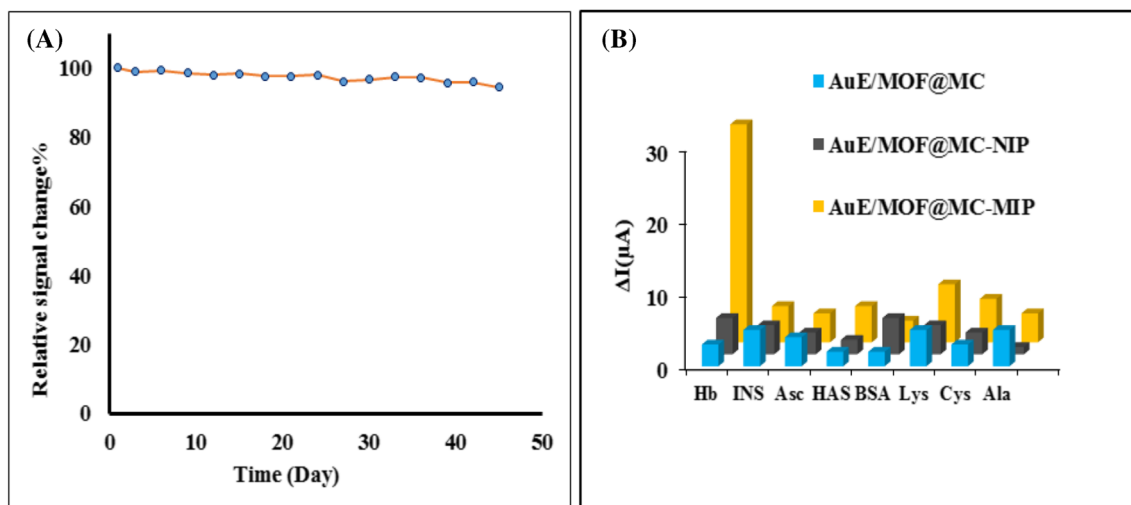


**Fig. 6** (a) Time dependence of relative current response change connecting to the original signal of the prepared AuE/MOF@MC-MIPs in a solution containing 10 mM  $[\text{Fe}(\text{CN})_6]^{3-/4-}$  (1:1) mixture and 0.1 M KCl, in PBS (pH = 6.0) with incubation time = 17.5 min, at 0.2 pM Hb on the first day of measurement. (b) Selectivity of AuE/MOF@MC-MIPs,

AuE/MOF@MC-NIPs, bare AuE, AuE/MOF, and AuE/MOF@MC for 0.2 pM Hb, 20 pM Asc, 20 pM HSA, 20 pM BSA, 20 pM INS, 20 pM Ala, and 20 pM Cys ( $n = 3$ ), in a solution containing 10 mM  $[\text{Fe}(\text{CN})_6]^{3-/4-}$  (1:1) mixture and 0.1 M KCl, in PBS (pH = 6) with incubation time = 17.5 min

**Table 3** Analytical parameters of the proposed sensing system using spiked human blood plasma samples

Analyte	Content ( $\mu\text{M}$ )	Added ( $\mu\text{M}$ )	Found ( $\mu\text{M}$ )	Recovery %	RSD % ( $n=5$ )
Hb	<sup>a</sup> $0.12 \times 10^{-4}$	$0.12 \times 10^{-4}$	$0.25 \times 10^{-4}$	104.20	4.5
		$0.24 \times 10^{-4}$	$0.35 \times 10^{-4}$	97.20	4.1
		$0.36 \times 10^{-4}$	$0.44 \times 10^{-4}$	95.65	5.1

<sup>a</sup> The content was determined by a blood test meter

placed adjacent to non-template MIPs, they can only interact through non-covalent bonding (Fig. S7). The selectivity of the AuE/MOF@MC-MIPs was evaluated using BSA, HSA, Ala, Lys, Cys, Asc, Lyz, and INS as competitive composites. The signal response of each protein on the AuE/MOF@MC-MIPs and AuE/MOF@MC-NIPs in a similar protein concentration (20 nM) estimated by DPV is shown in Fig. 6b. As observed, the response of the NIPs/AuE for Hb was much lower than that of AuE/MOF@MC-MIPs. This may be due to the complementary cavities of the imprinted layer, which increased the communication of Hb to the electrode surface, while the NIPs operated as a barrier between the electrode and the Hb. The DI values of the AuE/MOF@MC-NIPs towards Hb (30 mA) were 3.75, 10, 6, 4, 7.5, 5, 7.5 and 6 times the corresponding values for Lyz, BSA, INS, Asc, Cys, Ala and HSA, respectively. The results revealed that the Hb re-bound on AuE/MOF@MC-NIPs was much greater than that of the interfering proteins, and AuE/MOF@MC-NIPs demonstrated good selectivity for Hb. Furthermore, Hb displayed higher rebinding on MIPs than BSA, INS, Lyz, and HSA. Due to steric limitation, the larger proteins (BSA, INS, and HSA) were easier to remove from the imprinted holes, resulting in a weak signal response. On the contrary, the relatively higher response for Lyz may be ascribed to its much lower dimensions, allowing it to easily move into the imprinted holes and cause non-selective diffusion.

### Application of the sensor in blood samples

Analysis of real samples was carried out using the standard addition method in hemoglobin-spiked blood plasma samples

according to the literature [46, 47]. All blood samples were analyzed by a clinical blood test for sensing the Hb concentration, and the samples were then subjected to tenfold dilution and analyzed using the AuE/MOF@MC-MIPs, according to the proposed method. The results are reported in Table 3. As observed, the prepared AuE/MOF@MC-MIPs detected Hb with good recovery, which indicated that the designed AuE/MOF@MC-MIPs could be used for real samples. Three AuE/MOF@MC-MIPs organized under the same conditions were used. The Hb concentration was measured by DPV according to the procedure in section 3.2. Blood plasma samples were obtained from the Isfahan University of Technology Treatment Center.

### Conclusion

In summary, in this work, an Ag-MOF@MC-MIPs electrochemical biosensor for Hb has been introduced. The combined characteristics of mesoporous carbon and MOF enhance their catalytic properties significantly. In the presence of Hb, a barrier shell is created on the electrode surface. This restricts the possibility for electron transfer between the electrode and  $[\text{Fe}(\text{CN})_6]^{3-/4-}$  solution, which results in an increase in  $R_{\text{CT}}$  in EIS and a decrease in DPV peak current in the AuE/MOF@MC-MIPs. The probe performance was investigated in blood samples, and a maximum recovery rate of 99.02% was obtained, with  $\text{RSD}\% = 4.5\%$ , confirming the accuracy of the system. Therefore, the catalytic properties of Ag-MOF@MC were influential factors on the high sensitivity ( $\text{LOD} = 0.09 \text{ pM}$ ) of the developed biosensor. The system

**Table 4** Comparison of proposed Hb sensor (AuE/Ag-MOF@MC-MIPs) with other reported analytical sensors for detection of Hb

Sensor	Method	LDR	LOD	Ref.
Flow injection on screen printed electrode	Chronoamperometry	0.02–12.0 mg/mL	1.6 mg/ml	[48]
Graphene	Cyclic voltammetry	$1 \times 10^{-8}$ to $1 \times 10^{-2}$		[46]
Curcumin	Colorimetric	1–40, 50–150 $\mu\text{g}/\text{mL}$	0.1 $\mu\text{g}/\text{mL}$	[49]
Au nanoparticles	UV-Vis absorption	0.09–2.35 g/L	0.03 g/L	[50]
Au nanoflowers	Cyclic voltammetry	5–100 $\mu\text{g}/\text{mL}$	–	[51]
Ferrocenyl cysteine on screen printed electrode	Differential pulse voltammetry	0.1–1000 $\mu\text{g}/\text{mL}$	0.03 $\mu\text{g}/\text{mL}$	[52]
Single-walled carbon nanotube on screen printed electrode	Differential pulse voltammetry	–	0.03 $\mu\text{g}/\text{mL}$	[53]
ZnO nanoflowers	Differential pulse voltammetry	$1 \times 10^{-13}$ to $1 \times 10^{-1}$ mg/L	$3 \times 10^{-14}$ mg/L	[54]
AuE/Ag-MOF@MC-MIP	Differential pulse voltammetry	0.2 pM–1000 nM	0.09 pM	This work

revealed good selectivity when faced with a series of interferences. In addition, the Ag-MOF@MC-MIPs showed faster response time due to their higher mass transfer capability compared with Ag-MOF-MIPs, which is an important parameter for in situ observations. The sensor showed robustness and repeatability parameters at adequate levels. In contrast to similar electrochemical sensors for Hb, the developed sensor has good efficiency (Table 4).

**Supplementary Information** The online version contains supplementary material available at <https://doi.org/10.1007/s00216-021-03453-x>.

**Acknowledgements** The authors acknowledge the financial support from the Science Foundation of the Isfahan University of Technology, Center of Excellence in Sensors and Green Chemistry.

## Declarations

**Conflict of interest** The authors declare that there is no conflict of interest.

## References

- Trent JT, Watts RA, Hargrove MS. Human neuroglobin, a hexacoordinate hemoglobin that reversibly binds oxygen. *J Biol Chem.* 2001;276:30106–10.
- Roche CJ, Malashkevich V, Balazs TC, Dantsker D, Chen Q, Moreira J, et al. Structural and functional studies indicating altered redox properties of hemoglobin E IMPLICATIONS FOR PRODUCTION OF BIOACTIVE NITRIC OXIDE. *J Biol Chem.* 2011;286:23452–66.
- Vinogradov SN, Shlom JM, Kapp OH, Frossard P. The dissociation of annelid extracellular hemoglobins and their quaternary structure. *Comp Biochem Physiol B Biochem Mol Biol* 67(1980):1–16
- Wheby MS, Suttle GE, Ford KT. Intestinal absorption of hemoglobin iron. *Gastroenterology.* 1970;58:647–54.
- DeCarlo AA, Paramaesarvan M, Yun PL, Collyer C, Hunter N. Porphyrin-mediated binding to hemoglobin by the HA2 domain of cysteine proteinases (gingipains) and hemagglutinins from the periodontal pathogen *Porphyromonas gingivalis*. *J Bacteriol.* 1999;181:3784–91.
- Drain CM, Corden BB. Reversible oxygenation of oxygen transport proteins. *J Chem Educ.* 1987;64:441.
- Muncie HL Jr, Campbell JS. Alpha and beta thalassemia. *Am Fam Physician.* 2009;80:339–44.
- Walker I, Ali M. Hemoglobin abnormalities in neoplastic hematological disorders. *Can Med Assoc J.* 1973;108:843.
- Fucharoen S, Winichagoon P. Clinical and hematologic aspects of hemoglobin E  $\beta$ -thalassemia. *Curr Opin Hematol.* 2000;7:106–12.
- Fucharoen S, Weatherall DJ. Hemoglobin E disorders. *Disorders Hemoglobin.* 2009;5:417–33.
- Jetsrisuparb A, Sanchaisuriya K, Fucharoen G, Fucharoen S, Wiangnon S, Jetsrisuparb C, et al. Development of severe anemia during fever episodes in patients with hemoglobin E trait and hemoglobin H disease combinations. *Pediatr Hematol Oncol J.* 2006;28:249–53.
- Lette G, Sankaran VG, Bezerra MAC, Araújo AS, Uda M, Sanna S, et al. DNA polymorphisms at the BCL11A, HBS1L-MYB, and  $\beta$ -globin loci associate with fetal hemoglobin levels and pain crises in sickle cell disease. *Proc Natl Acad.* 2008;105:11869–74.
- Zollinger A, Hager P, Singer T, Friedl HP, Pasch T, Spahn DR. Extreme hemodilution due to massive blood loss in tumor surgery. *J ASA.* 1997;87:985–7.
- Kleinert P, Schmid M, Zurbriggen K, Speer O, Schmutz M, Roschitzki B, et al. Mass spectrometry: a tool for enhanced detection of hemoglobin variants. *Clin Chem.* 2008;54:69–76.
- Fang L, Li W, Zhou Y, Liu C-C. A single-use, disposable iridium-modified electrochemical biosensor for fructosyl valine for the glycosylated hemoglobin detection. *Sensors Actuators B Chem.* 2009;137:235–8.
- Wolf U, Wolf M, Choi JH, Levi M, Choudhury D, Hull S, et al. Localized irregularities in hemoglobin flow and oxygenation in calf muscle in patients with peripheral vascular disease detected with near-infrared spectrophotometry. *Eur J Vasc Endovasc Surg.* 2003;37:1017–26.
- Kutlar F, Kutlar A, Huisman T. Separation of normal and abnormal hemoglobin chains by reversed-phase high-performance liquid chromatography. *J Chromatogr A.* 1986;357:147–53.
- Yang X-F, Guo X-Q, Li H. Fluorimetric determination of hemoglobin using spiro form rhodamine B hydrazide in a micellar medium. *Talanta.* 2003;61:439–45.
- Cormack PA, Elorza AZ. Molecularly imprinted polymers: synthesis and characterisation. *J Chromatogr B.* 2004;804:173–82.
- Wulff G. Molecular imprinting in cross-linked materials with the aid of molecular templates—a way towards artificial antibodies. *Angew Chem Int Ed.* 1995;34:1812–32.
- Stobiecka M, Hepel M. Effect of buried potential barrier in label-less electrochemical immunodetection of glutathione and glutathione-capped gold nanoparticles. *Biosens Bioelectron.* 2011;26:3524–30.
- Dickert FL, Hayden O. Imprinting with sensor development—on the way to synthetic antibodies. *J Anal Chem.* 1999;364:506–11.
- Haupt K, Mosbach K. Plastic antibodies: developments and applications. *Trends Biotechnol.* 1998;16:468–75.
- Guo Z, Florea A, Jiang M, Mei Y, Zhang W, Zhang A, et al. Molecularly imprinted polymer/metal organic framework based chemical sensors. *Coating.* 2016;6:42.
- Li J, Wang X, Zhao G, Chen C, Chai Z, Alsaedi A, et al. Metal-organic framework-based materials: superior adsorbents for the capture of toxic and radioactive metal ions. *Chem Soc Rev.* 2018;47:2322–56.
- Khan NA, Hasan Z, Jung SH. Adsorptive removal of hazardous materials using metal-organic frameworks (MOFs): a review. *J Hazard Mater.* 2013;244:444–56.
- Ameloot R, Stappers L, Franssaer J, Alaerts L, Sels BF, De Vos DE. Patterned growth of metal-organic framework coatings by electrochemical synthesis. *Chem Mater.* 2009;21:2580–2.
- Lee J, Farha OK, Roberts J, Scheidt KA, Nguyen ST, Hupp JT. Metal-organic framework materials as catalysts. *Chem Soc Rev.* 2009;38:1450–9.
- Yot PG, Vanduyfhuys L, Alvarez E, Rodriguez J, Itié J-P, Fabry P, et al. Mechanical energy storage performance of an aluminum fumarate metal-organic framework. *Chem Sci.* 2016;7:446–50.
- Chen B, Yang Y, Zapata F, Lin G, Qian G, Lobkovsky EB. Luminescent open metal sites within a metal-organic framework for sensing small molecules. *J Adv Mater.* 2007;19:1693–6.
- Prasad K, Bazaka O, Chua M, Rochford M, Fedrick L, Spoor J, et al. Metallic biomaterials: current challenges and opportunities. *Materials.* 2017;10:884.
- Coudert F-X, Fuchs AH. Computational characterization and prediction of metal-organic framework properties. *Coord Chem Rev.* 2016;307:211–36.
- Ding B, Liu SX, Cheng Y, Guo C, Wu XX, Guo JH, et al. Heterometallic alkaline earth-lanthanide BaII-LaIII microporous metal-organic framework as bifunctional luminescent probes of Al<sup>3+</sup> and MnO<sub>4</sub>. *Inorg Chem.* 2016;55:4391–402.

34. Cao J, Gao Y, Wang Y, Du C, Liu Z. A microporous metal–organic open framework containing uncoordinated carbonyl groups as postsynthetic modification sites for cation exchange and Tb 3+ sensing. *Chem Commun.* 2013;49:6897–9.
35. Zhao Y, Wu H, Emge TJ, Gong Q, Nijem N, Chabal YJ, et al. Enhancing gas adsorption and separation capacity through ligand functionalization of microporous metal–organic framework structures. *Chem Eur J.* 2011;17:5101–9.
36. Bougrini M, Florea A, Cristea C, Sandulescu R, Vocanson F, Errachid A, et al. Development of a novel sensitive molecularly imprinted polymer sensor based on electropolymerization of a microporous-metal-organic framework for tetracycline detection in honey. *Food Control.* 2016;59:424–9.
37. Li M, Sun P, Wu Q, Liu D, Zhou L. Core–shell magnetic metal–organic framework molecularly imprinted nanospheres for specific adsorption of tetrabromobisphenol A from water. *Environ Sci Nano.* 2018;5:2651–62.
38. Lu C, Ben T, Xu S, Qiu S. Electrochemical synthesis of a microporous conductive polymer based on a metal–organic framework thin film. *Angew Chem Int Ed.* 2014;53:6454–8.
39. Qian K, Fang G, Wang S. A novel core–shell molecularly imprinted polymer based on metal–organic frameworks as a matrix. *Chemical Comm.* 2011;47:10118–20.
40. Khan S, Wong A, Zaroni MVB, Sotomayor MDPT. Electrochemical sensors based on biomimetic magnetic molecularly imprinted polymer for selective quantification of methyl green in environmental samples. *Mater Sci Eng C.* 2019;103:109825.
41. Rico-Yuste A, Carrasco S. Molecularly imprinted polymer-based hybrid materials for the development of optical sensors. *Polymers.* 2019;11:1173.
42. Yadav DK, Ganesan V, Marken F, Gupta R, Sonkar PK. Metal@MOF materials in electroanalysis: silver-enhanced oxidation reactivity towards nitrophenols adsorbed into a zinc metal organic framework—ag@MOF-5 (Zn). *Electrochim Acta.* 2016;219:482–91.
43. Liu J, Strachan DM, Thallapally PK. Enhanced noble gas adsorption in ag@MOF-74Ni. *Chem Comm.* 2014;50:466–8.
44. Piletsky S, Panasyuk T, Piletskaya E, Nicholls IA, Ulbricht M. Receptor and transport properties of imprinted polymer membranes—a review. *J Membr Sci.* 1999;157:263–78.
45. Sun D, Cao R, Bi W, Weng J, Hong M, Liang Y. Syntheses and characterizations of a series of silver-carboxylate polymers. *Inorganica Chim Acta.* 2004;357:991–1001.
46. Sun Y, Lan Y, Yang L, Kong F, Du H, Feng C. Preparation of hemoglobin imprinted polymers based on graphene and protein removal assisted by electric potential. *RSC Adv.* 2016;6:61897–905.
47. Wang Z, Li F, Xia J, Xia L, Zhang F, Bi S, et al. An ionic liquid-modified graphene based molecular imprinting electrochemical sensor for sensitive detection of bovine hemoglobin. *Biosens Bioelectron.* 2014;61:391–6.
48. Liu A, Xu S, Deng H, Wang X. A new electrochemical HbA1c biosensor based on flow injection and screen-printed electrode. *Int J Electrochem Sci.* 2016;11:3086–94.
49. Pourreza N, Golmohammadi H. Hemoglobin detection using curcumin nanoparticles as a colorimetric chemosensor. *RSC Adv.* 2015;5:1712–7.
50. Thea R, Onna D, Kreuzer MP, Hamer M. Label-free nanostructured sensor for the simple determination of glycosylated hemoglobin (HbA1c). *Sens Actuators B Chem.* 2019;297:126722.
51. Wang X, Su J, Zeng D, Liu G, Liu L, Xu Y, et al. Gold nanoflowers (Au NFs) modified screen-printed carbon electrode electrochemical biosensor for label-free and quantitative detection of glycosylated hemoglobin. *Talanta.* 2019;201:119–25.
52. Han G-C, Su X, Hou J, Ferranco A, Feng X-Z, Zeng R, et al. Disposable electrochemical sensors for hemoglobin detection based on ferrocenyl cysteine conjugates modified electrode. *Sens Actuators B Chem.* 2019;282:130–6.
53. Eissa S, Almusharraf AY, Zourob M. A comparison of the performance of voltammetric aptasensors for glycosylated haemoglobin on different carbon nanomaterials-modified screen printed electrodes. *Mater Sci Eng C.* 2019;101:423–30.
54. Sun Y, Li S, Yang Y, Feng X, Wang W, Liu Y, et al. Fabrication of a thermal responsive hemoglobin (Hb) biosensor via Hb-catalyzed eATRP on the surface of ZnO nanoflowers. *J Electroanal Chem.* 2019;848:113346.

**Publisher's note** Springer Nature remains neutral with regard to jurisdictional claims in published maps and institutional affiliations.